Development of flux-tuneable inductive nanobridge SQUIDs for quantum technology applications

Laith Meti, George Long, Tom Godfrey, Jamie Potter, David Cox, Gemma Chapman, John Gallop, Edward Romans, and Ling Hao

***Abstract*—Niobium nanobridge SQUIDs have shown exceptional noise performance with potential applications in quantum information processing, weak signal detection and single spin detection where the nanobridge geometry should enable efficient electromagnetic coupling to implanted spins. Combining such devices with dispersive microwave readout circuitry allows the spin sensitivity to be further improved by overcoming the standard thermal limit. Here we report on the fabrication and dispersive microwave readout of an array of niobium nanobridge rf SQUIDs incorporated into a superconducting resonator, including the optimization of the nanobridge fabrication process by electron beam lithography. We show the measured flux-tuneability of the resonance is in good agreement with theory, and we also discuss how the nonlinearity of the weak-link in the resonator structure allows for the mediation of parametric effects to enhance performance.**

***Index Terms*—Electron beam lithography (EBL), nanoscale superconducting quantum interference devices (nanoSQUIDs), co-planar waveguide resonators (CPW), three wave mixing (3WM), parametric amplification.**

I. Introduction

Recently there has been considerable effort in developing both nanoscale Superconducting Quantum Interference Devices (nanoSQUIDs), and also in embedding SQUIDs in superconducting resonator structures allowing the development of various microwave/rf readout and amplification techniques [1]-[4]. Various types of nanoSQUIDs are being developed towards single spin detection type applications in quantum computing/information processing, quantum error correction, quantum metrology, materials science and nano-biology [5]-[8]. Although other single spin detection technologies are also being developed, e.g. nitrogen-vacancies in diamond [9], optical to phonon semiconducting materials [10] and solid state sensors [11], these generally involve long integration times [12] to achieve true single spin resolution. This presents an obstacle for applications involving short coherence times (e.g. spin-based qubits) or where real-time monitoring of spin systems on sub-second timescales is required [3].

In contrast the inherent sensitivity of nanoSQUIDs can potentially overcome this limitation. Recently we have demonstrated Nb nanobridge SQUIDs fabricated with nano-constrictions with lengths comparable to the Ginzburg-Landau coherence length $\xi(T) \sim 40$ nm at 4.2 K [14]. Operated conventionally in the voltage state, the equivalent flux noise of such devices translates into a theoretical spin sensitivity (in terms of the Bohr magneton) of $\sim 10\,\mu_B/\sqrt{\mathrm{Hz}}$ at 4.2 K [15] and $\sim 0.29\,\mu_B/\sqrt{\mathrm{Hz}}$ at mK temperatures [16].

In principle this spin sensitivity can be further improved upon by employing a non-dissipative readout where the nanobridge SQUID is used as a flux-tuneable non-linear inductor in the superconducting state which then overcomes the standard thermal noise limit [17]. This could be achieved by incorporating the SQUID into a discrete *LC*-circuit [2] or by embedding the SQUID into a thin-film superconducting resonator structure [1]. Well below the critical temperature T_c, such resonators can have a high internal quality factor Q_i due to the low density of lossy quasi-particles. The overall loaded quality factor is then controlled by the coupling capacitors [18], giving great freedom to tailor the overall Q for different applications.

In this paper we build upon our previous work [19] by embedding an array of rf nanobridge SQUIDs into superconducting co-planar waveguide (CPW) resonators to increase the non-linear response and thus the flux sensitivity [20][21]. Section II introduces the analytic theory of rf nanobridge SQUIDS embedded in CPW resonators, and Section III presents simulations showing the additional potential for exploiting parametric amplification. Section IV describes the fabrication and characterisation of devices fabricated by electron-beam lithography, and we demonstrate tailoring of the electron-beam process to produce devices with reduced critical currents in order to keep the rf SQUID screening parameter $\beta_l < 1$. Section V discusses the microwave readout measurements, and finally we present our conclusions and comment on potential future work.

II. Theory

An rf SQUID is a continuous superconducting loop that is interrupted by a single Josephson junction/weak-link. Due to the quantum nature of superconductivity, the phase change in

Revised manuscript received 28th Jan 2023. This work was supported by UKRI (ST/T006099/1) and the UK NMS. For the purpose of open access, the author(s) has applied a CC BY license to any Accepted Manuscript version arising.

Laith Meti (corresponding author, e-mail: laith.meti.19@ucl.ac.uk) and Tom Godfrey are with NPL, Teddington TW11 0LW, UK, and also with the London Centre for Nanotechnology, UCL, London WC1H 0AH, UK.

George Long, Jamie Potter, Gemma Chapman, John Gallop, and Ling Hao are with NPL, Teddington TW11 0LW, UK.

David Cox is with NPL, Teddington TW11 0LW, UK, and also with the University of Surrey, Guildford GU2 7XH, UK.

Edward Romans is with LCN, UCL, London WC1H 0AH, UK.

the superconducting wavefunction across the junction/weak-link can be shown to satisfy:

$$\phi = 2\pi m - 2\pi\Phi/\Phi_0\,, \tag{1}$$

where Φ is the flux inside the loop, $\Phi_0 = h/(2e)$ is the flux quantum, and m is an integer. Differentiating this leads to the second Josephson equation:

$$d\phi/dt \;=\; U \cdot 2\pi/\Phi_0\,, \tag{2}$$

where U is the potential difference across the junction. Differentiating the first Josephson equation: $I = I_c \sin(\phi)$ and using (2) we arrive at the non-linear Josephson inductance:

$$L_J = \Phi_0/(2\pi I_c \cos(\phi)). \tag{3}$$

If we also consider the geometrical inductance L_g of the loop, the total parallel inductance satisfies:

$$1/L_T = 1/L_J + 1/L_g, \text{ or} \tag{4a}$$
$$L_T = L_g/(1 + \beta_L \cos(\phi)), \tag{4b}$$

where we have introduced the SQUID screening parameter $\beta_l = 2\pi L_g I_c/\Phi_0$. For an array of N such rf SQUIDs embedded into a $\lambda/2$ CPW superconducting resonator, the intrinsic resonant frequency of the resonator is perturbed to:

$$f = 1/\,2\sqrt{(L_{res} + NL_T)C_{res}}\,, \tag{5}$$

where L_{res} and C_{res} are the total inductance and capacitance of the resonator. There is a trade-off in device design between having a large resonant shift for large L_g and having non-hysteretic behaviour and low noise sensitivity for small L_g [22]. For a single embedded rf SQUID ($N = 1$) with parameters corresponding to the 1.072 GHz resonator demonstrated in Section V, (5) predicts a maximum center frequency shift of ~ 14 kHz using values of L_{res} and C_{res} estimated by standard elliptical integral expressions for CPW structures.

The embedding of an rf SQUID also leads to the possibility of exploiting parametric amplification. In the presence of both an injected ac current from the resonator and a dc magnetic flux Φ_{DC} in the loop from an external field, we can explicitly redefine $\phi \rightarrow \phi_{AC} + \phi_{DC}$ where $\phi_{DC} = 2\pi\Phi_{DC}/\Phi_0$. For nanobridges the shunt capacitance can be neglected so from Kirchhoff's current law the total current through the two parallel branches of the rf SQUID [23]-[25] is :

$$I = I_J + I_L\,, \tag{7a}$$
$$I = I_c \sin(\phi) + 1/L_g \int U_L\,, \tag{7b}$$
$$I = I_c \sin(\phi_{AC} + \phi_{DC}) + \phi_{AC}\Phi_0/2\pi L_g - I_c \sin(\phi_{DC}), \tag{7c}$$

where the last term is an integration constant corresponding to the circulating current.

Generally, $\phi_{AC} \ll \phi_{DC}$, and in this limit it is sufficient to expand (7c) to third order as:

$$I/I_c = [\cos(\phi_{DC}) + \beta_l^{-1}]\,\phi_{AC} - \alpha\,\phi_{AC}^2 - \gamma\phi_{AC}^3 \tag{8}$$

where $\alpha = 1/2\sin(\phi_{DC})$ and $\gamma = 1/6\cos(\phi_{DC})$. The magnitudes of these coefficients are plotted below in Fig. 1. When α is maximum and γ is zero, a purely 3-wave mixing (3WM) regime is encountered where $\hbar\omega_1 + \hbar\omega_2 = \hbar\omega_3$ [26][27]. Conversely when γ is maximum and α is zero a purely 4-wave mixing (4WM) regime is encountered where $\hbar\omega_1 + \hbar\omega_2 = \hbar\omega_3 + \hbar\omega_4$. Using wave-mixing interactions mediated via the nonlinearity of the SQUID allows for these devices to exploit parametric amplification to enhance readout via transferring energy between the coupled modes satisfying the frequency matching conditions for the chosen mixing regime, e.g. the pump tone to the signal tone.

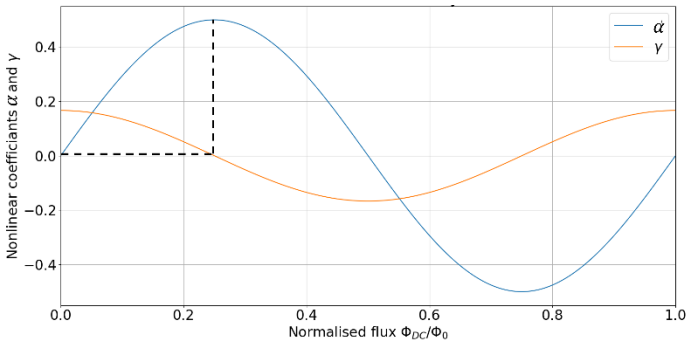

Fig. 1. Nonlinear coefficients of Equation (8) plotted for one normalised period of applied flux. The dashed line indicates a purely 3-wave mixing regime where the quadratic term is maximum, and the cubic term vanishes.

III. Simulation

As an example of the 3WM behavior we modelled the circuit shown Fig. 2 using the simulation package WRspice [28]. The circuit represents a $\lambda/2$ CPW superconducting resonator as lossless transmission lines [29] with each end capacitively coupled to input and output ports. An rf SQUID is embedded one third of the way across the resonator and its geometric inductance is mutually-coupled to a flux-bias circuit.

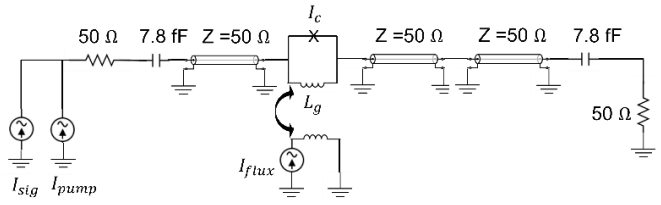

Fig. 2. Circuit schematic of the WRspice model for an rf SQUID embedded a third of the way across a $\lambda/2$ CPW resonator. The coupling capacitors provide the node conditions and the superconductor resonator is modelled by three lossless transmission line elements. The external applied flux threading the SQUID is provided by a separate bias circuit.

As explained above the pump current needs to be kept small but eventually as the pump current is increased the assumption that $\phi_{AC} \ll \phi_{DC}$ starts to break down. This means we must keep

the pump current relatively small to achieve 3WM. This is checked in WRspice by measuring the junction phase versus the applied flux. For 3WM, nondegenerate frequency matching constraints must be satisfied such that a pump applied at $\sim 2f_s$ can mix with photons in the primary tone f_s and generate an idler detuned around f_s, i.e. $f_i + f_s = f_p \approx 2f_s$. In experimental realisation, the pump tone at $2f_s$ is far removed from the signal band and can be removed via low pass filtering. To realise this experimentally, the rf SQUID must be embedded in a location where it can strongly couple to the pump tone at the second harmonic $2f_s$. This is achieved by choosing the location of the rf SQUID along the resonator. For $\lambda/2$ resonators the SQUID should be embedded a third of the way along the resonator. For $\lambda/4$ resonators the position would be halfway along the resonator.

The frequency response of the resonator as a function of pump current was simulated for a 6 GHz resonator with the geometrical SQUID loop inductance set to 12 pH and the junction critical current set to $I_c = 5$ μA with $\beta_l \sim 0.2$. A signal tone ($f_s = 5.92$ GHz, $I_{sig} = 0.1$ μA) and a pump tone ($f_p = 12$ GHz) is injected into the resonator. The output of the resonator in the frequency domain is determined by taking an FFT of the time-varying voltage across the 50 Ω termination resistor for varying pump tone amplitudes (0–2μA). Fig. 3 shows the relative amplitude of the simulated resonance peak compared to the no pump case ($I_p = 0$ μA). The enhancement in the resonant amplitude is approaching 13 dB which can be further improved by incorporating an array of rf SQUIDs into the resonator.

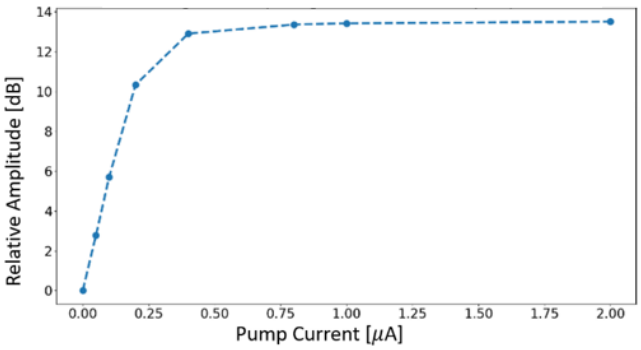

Fig. 3. The relative amplitude of the simulated resonance peak compared to the no pump case is plotted as a function of pump current. The amplitude saturates for $I_p > 0.5$ μA.

IV. Fabrication and DC Characterization

In the present work we fabricated Nb nanobridges using electron beam lithography (EBL) followed by reactive ion etching (RIE). Each chip contained both a superconducting resonator structure with embedded rf SQUIDs and a set of autonomous dc SQUID test structures incorporating equivalent nanobridges to allow the nanobridge electrical parameters to be easily determined. Typical devices are shown in Fig. 4.

The fabrication procedure is as follows: 300 nm 950 PMMA A4 photoresist was spun onto a ~150 nm-thick sputtered Nb film on an 8 mm x 8 mm silicon substrate and baked at 180 ºC for 90 s. Nanobridges and fine-feature structures were written with a 300 pA electron beam current from a 100 keV source. Coarse structures were simultaneously written in the same exposure-run with a 20 nA beam current. In both writing steps appropriate proximity effect corrections were made with more isolated larger features like bond pads dosed less (~600 μC/μm^2), and more populated write fields and nanobridges dosed significantly more (~1300 μC/μm^2). The exposed sample was then developed at room temperature with a 3:1 IPA: MIBK developer for 105 seconds followed by a 4-minute CH_3: SF_6 reactive ion etch (RIE). For the initial set of device chips fabricated, the nanobridges were all imaged to be 90 nm long by 50 nm wide as can be seen for a dc SQUID in Fig. 4(b).

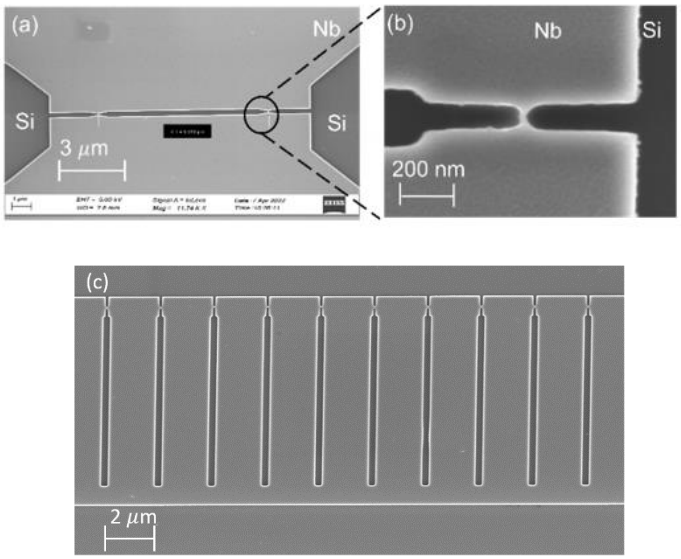

Fig. 4. (a) SEM image of a dc SQUID test structure made by EBL. Both nanobridges are ~90 nm long by ~50 nm wide. (b) SEM image showing one of the nanobridges in more detail. (c) Example of 10 nanobridge rf SQUIDs embedded into the center conductor of a $\lambda/2$ CPW resonator.

Fig. 5(a) shows the measured current-voltage characteristics of this dc SQUID and as can be seen the nanobridges have a critical temperature of ~8.6 K close to the T_c of the bulk film (~8.9 K). In contrast we find for nanobridges fabricated by focused ion-beam (FIB) that there is often a suppression in the junction T_c that is likely because of ion-implantation in the FIB process [30][31].

The very large critical currents for the EBL nanobridges lead to the generation of significant Joule heating in the voltage state which leads them to exhibit thermal hysteresis [34] except very close to T_c. For inductive readout in the superconducting state this thermal hysteresis is not an issue. However, this critical current was too large to ensure $\beta_l < 1$ for an embedded rf SQUID and so we needed to reduce it. To achieve this, we refined our EBL process to further improve the minimum resolution achievable. This involved a 'bulk and sleeve' approach [32] specific to our particular EBL exposure method for regions where the fine-feature SQUID structures merge into the large-feature resonator structure. Here the inner 2 μm of the large feature is fragmented into sleeves with a 300 pA beam current (~ 1100 μC/μm^2). This enabled us to realise nanobridges that were 90 nm long by only 20 nm wide.

This article has been accepted for publication in IEEE Transactions on Applied Superconductivity. This is the author's version which has not been fully edited and content may change prior to final publication. Citation information: DOI 10.1109/TASC.2023.3244771

The current-voltage characteristics of a dc SQUID with 20 nm-wide nanobridges are shown in Fig. 5(b) showing the reduced critical current compared to the 50 nm-wide nanobridge device. From previous studies [33] we find the typical on-chip variation in critical currents of EBL nanobridges is reasonably small ~17% with a high yield. Ignoring any asymmetry in the dc SQUID we estimate the likely critical current of embedded rf SQUIDs on the same chip will be ~250 μA at the base temperature of our system (~3.5 K). This makes them feasible for operation at that temperature whilst keeping $\beta_l < 1$.

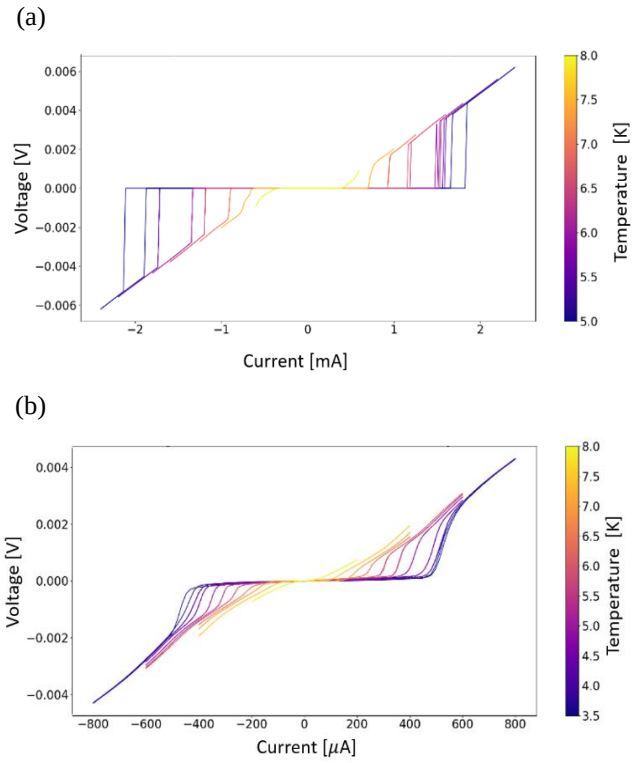

Fig. 5. (a) Typical current–voltage curves versus temperature for a dc test SQUID with 90 nm x 50 nm EBL nanobridges. (b) Typical current–voltage curves versus temperature for a dc test SQUID with 90 nm x 20 nm nanobridges following refinement of the EBL process giving a reduced SQUID critical current of ~ 500 μA at 3.5 K.

V. Inductive Readout

To realize inductive readout of superconducting resonators, a CPW geometry was chosen to define the resonant structures. A range of rf-SQUID embedded devices with resonant frequencies from 1-7 GHz were fabricated with either a single $\lambda/2$ CPW resonator per chip or multiple $\lambda/4$ CPW resonators capacitively coupled to a common feedline. Some devices had an additional control line for on-chip flux bias. The resonator chip was housed in a copper sample enclosure with a highly attenuated input line and an amplified (cryogenic HEMT amplifier) output line, to allow for connection to room temperature measurement equipment.

Fig. 6(a) shows an $|S_{21}|$ measurement at 3.5 K of a $\lambda/2$ CPW resonator with an embedded array of ten rf SQUIDs (N = 10) with a fundamental frequency of 1.072 GHz. N = 10 was chosen to give a significant enhancement in the resonant shift but with a high probability that all of the rf SQUIDs in the array would be working. Each rf SQUID had an estimated L_g ~ 1.216 pH (estimated using the software package 3D-MSLI [34][35]). The measured Q-factor at 3.5 K was 909. This device was fabricated from a fairly old film and the etch time during its fabrication had not been optimized. We have recently achieved higher Q ~ 9000-15000 at 3.5 K in several devices utilising newer films with minimized etch times, although the exact reason for the improvement is still unknown.

The center frequency shift measured as a function of applied field for the N = 10 device is plotted in Fig. 6(b), together with a fit using (5). The extracted critical current for each nanobridge is 258 μA which is in good agreement with our estimate from the dc SQUID measurements on the same chip and implies the rf SQUIDs have β_l = 0.95.

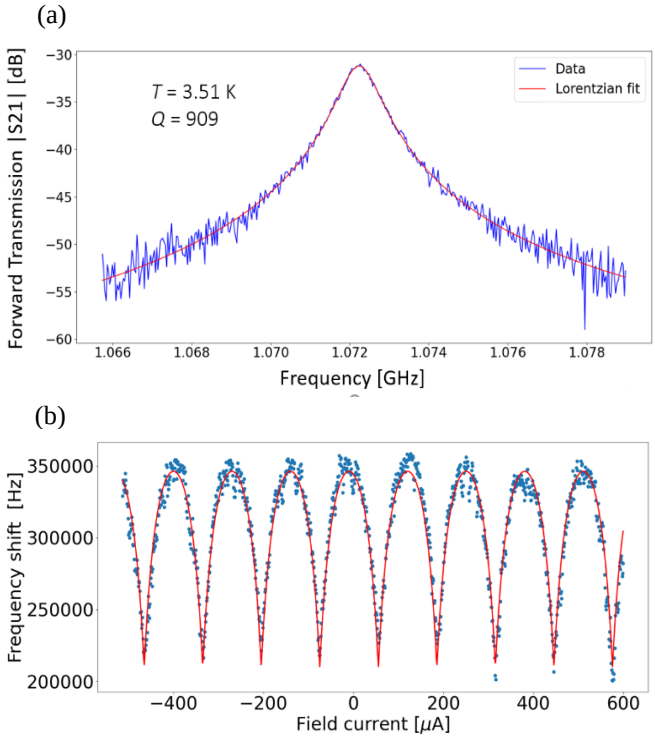

Fig. 6. (a) Example of a Lorentzian fit to the first harmonic at 1.072 GHz of an EBL rf SQUID array (N = 10) embedded centrally in a $\lambda/2$ resonator. (b) Measured center frequency shift as a function of applied flux over a wide range of periods. The measured data is shown in blue, and a fit to the data using (5) is shown in red for a fitted nanobridge critical current of 258 μA.

VI. Conclusion

We have demonstrated the ability to fabricate Nb nanobridges with widths down to ~ 20 nm giving a sufficiently low critical current at 3.5 K for use in CPW resonators with embedded arrays of rf SQUIDs. We have successfully shown that such devices operate as a flux tunable resonator with good agreement between the frequency shift and theory. Our next step is to work towards implanting a spin cluster onto our nanobridge loop for spin detection experiments. We have also simulated a 3WM regime of our resonators which we expect to lead to further work on parametric amplification.

REFERENCES

[1] O.W. Kennedy, J. Burnett, J.C. Fenton, N.G.N. Constantino, P.A. Warburton, J.J.L. Morton, and E. Dupont-Ferrier, "Tunable Nb superconducting resonator based on a constriction nano-SQUID fabricated with a Ne focused ion beam," *Phys. Rev. Appl.*, vol. 11, no. 1, 2019, Art. no. 014006.

[2] E. M. Levenson-Falk, R. Vijay, N. Antler, and I. Siddiqi, "A dispersive nanoSQUID magnetometer for ultra-low noise, high bandwidth flux detection," *Supercond. Sci. Technol*., vol. 26, no. 5, 2013, Art. no. 055015.

[3] M. Sandberg et al., "Tuning the field in a microwave resonator faster than the photon lifetime," *Appl. Phys. Lett.*, vol. 92, no. 20, 2008, Art. no. 203501.

[4] D. A. Bennett., J. A. Mates, J. D. Gard, A. S. Hoover, M. W. Rabin, C. D. Reintsema, D. R. Schmidt, L. R. Vale, and J. N. Ullom, "Integration of TES microcalorimeters with microwave SQUID multiplexed readout," *IEEE Trans. Appl. Supercond.*, vol. 25, no. 3, 2014, pp.1-5.

[5] L. C. L. Hollenberg, C. J. Wellard, C. I. Pakes, and A. G. Fowler,"Single-spin readout for buried dopant semiconductor qubits," *Physical Review B*, vol. 69, no. 23, 2004, p.233301.

[6] F. Kalhor, L. Yang, L. Bauer, and Z. Jacob, "Quantum sensing of photonic spin density using a single spin qubit", *Physical Review Research*, vol. 3, no. 4, 2021, p.043007.

[7] H. Zhou et al., "Quantum metrology with strongly interacting spin systems", *Physical review X*, vol. 10, no. 3, 2020, p.031003.

[8] M. Pelliccione et al., "Scanned probe imaging of nanoscale magnetism at cryogenic temperatures with a single-spin quantum sensor", *Nature nanotechnology*, vol. 11, no. 8, 2016, p.70.

[9] D. Suter, and, F. Jelezko, "Single-spin magnetic resonance in the nitrogen-vacancy center of diamond", *Progress in nuclear magnetic resonance spectroscopy*, vol. 98, 2017, pp.50-62.

[10] R. Vrijen and E. Yablonovitch, "A spin-coherent semiconductor photodetector for quantum communication", *Physica E: Low-dimensional Systems and Nanostructures*, vol. 10, no. 4, 2001. pp.569-575.

[11] W. B. Gao, A. Imamoglu, H. Bernien, R. Hanson, "Coherent manipulation, measurement and entanglement of individual solid-state spins using optical fields", *Nature Photonics*, vol. 9, no.6, 2015, pp.363-373.

[12] M. S. Grinolds, S. Hong, P. Maletinsky, L. Luan, M. D. Lukin, R. L. Walsworth & A. Yacoby, "Nanoscale magnetic imaging of a single electron spin under ambient conditions", *Nature Physics*, vol. 9, no.4, 2013, pp.215-219.

[13] M. Atatüre, D. Englund, N. Vamivakas, and S. Lee, "Material platforms for spin-based photonic quantum technologies". *Nature Reviews Materials.*, vol.3, vo. 5, 2018, pp. 38–51.

[14] L. Hao, J. C. Macfarlane, J. C. Gallop, E. Romans, D. Cox, D. Hutson, and J. Chen, "Spatial resolution assessment of Nano-SQUIDs made by focused ion beam", *IEEE transactions on applied superconductivity*, vol. 17, no.2, 2007, pp.742-745.

[15] E. Romans et al., "Noise performance of niobium Nano-SQUIDs in applied magnetic fields", *IEEE transactions on applied superconductivity*, vol. 21, no. 3 , 2011, pp.404-407.

[16] Y. Anahory et al., "SQUID-on-tip with single-electron spin sensitivity for high-field and ultra-low temperature nanomagnetic imaging", *Nanoscale*, vol. 12, no. 5, 2020, pp.3174-3182.

[17] F. Wulschner et al. , "Tunable coupling of transmission-line microwave resonators mediated by an rf SQUID", EPJ Quantum Technology, vol. 3, no. 1, 2016, pp.1-10.

[18] M. Göppl, A. Fragner, M. Baur, R. Bianchetti, S. Filipp, J. M. Fink, P. J. Leek, G. Puebla, L. Steffen, and A. Wallraff, "Coplanar waveguide resonators for circuit quantum electrodynamics", *Journal of Applied Physics*, vol. 104, no.11, 2008, p.113904.

[19] T. Godfrey et al., "Microwave Inductive Readout of EBL Nanobridge SQUIDs", *IEEE Transactions on Applied Superconductivity*, vol. 30, no.7, 2020 , pp.1-4.

[20] A. V. Ustinov, "Experiments With Tunable Superconducting Metamaterials", *IEEE Transactions on Terahertz Science and Technology*, vol. 5, no. 1, 2015, pp. 22-26.

[21] M. A. Castellanos-Beltrana, and K. W. Lehnert, "Widely tunable parametric amplifier based on a superconducting quantum interference device array resonator", *Appl. Phys. Lett*, vol. 91, 2007, Art. No. 083509.

[22] M. B. Ketchen, D. D. Awschalom, W. J. Gallagher, A. W. Kleinsasser, R. L. Sandstrom, J. R. Rozen, and B. Bumble, "Design, fabrication, and performance of integrated miniature SQUID susceptometers", *IEEE Transactions on Magnetics*, vol. 25, no.2, 1989, pp.1212-1215.

[23] M. M. Müller, B. Maier, C. Rockstuhl and M. Hochbruck, "Analytical and numerical analysis of linear and nonlinear properties of an rf-SQUID based metasurface", *Physical Review B*, vol. 99, no. 7, 2019 , p.075401.

[24] O. Yaakobi, L. Friedland, C. Macklin, and I. Siddiqi, "Parametric amplification in Josephson junction embedded transmission lines", *Physical Review B*, vol. 87, no. 14, 2013, p.144301.

[25] S. M. Frolov, *PhD Thesis:* "*Current-phase relations of Josephson junctions with ferromagnetic barriers"*, University of Illinois at Urbana-Champaign, 2005.

[26] T. Dixon, J. W. Dunstan, G. B. Long, J. M. Williams, P.J Meeson, and C.D. Shelly, "Capturing complex behavior in Josephson traveling- wave parametric amplifiers", *Physical Review Applied*, vol. 14, no. 3, 2020, p.034058.

[27] A.B Zorin, "Josephson traveling-wave parametric amplifier with three-wave mixing", *Physical Review Applied*, vol. 6, no. 3, 2016, p.034006.

[28] IC Design Software for Unix/Linux and Windows Whiteley Research Inc., 456 Flora Vista Avenue, Sunnyvale CA 94086.

[29] D. M. Pozar, Micro. Eng., 4th ed. Hoboken, NJ, USA: Wiley, 2011.

[30] T. Godfrey, J. C. Gallop, D. C. Cox E. J. Romans, J. Chen, and L. Hao, "Investigation of dayem bridge NanoSQUIDs made by Xe focused ion beam". *IEEE Transactions on Applied Superconductivity*, vol. 28, no. 7, 2018, pp.1-5.

[31] E. Polychroniou, J. Gallop, T. Godfrey, D. Cox, G. Long, J. Chen, E. Romans, and L. Hao, "Investigation of NanoSQUIDs Fabricated with a Range of Focused Ion Beam Sources", *Journal of Physics: Conference Series*, vol. 1559, no. 1, 2020, p. 012015.

[32] W.J. Skocpol, M.R. Beasley, and M. Tinkham, "Self-heating hotspots in superconducting thin-film microbridges", *Journal of Applied Physics*, vol. 45, no. 9, 1974, pp.4054-4066.

[33] For details about the bulk and sleeve technique we used see https://www.genisys-gmbh.com/advanced-exposure-technique.html

[34] C. D. Shelly, P. See, J. Ireland, E. J. Romans and J. M. Williams, "Weak link nanobridges as single flux quantum elements," *Supercond. Sci. Technol.* vol. 30, 2017, p.095013.

[35] M.M. Khapaev, A.Yu. Kidiyarova-Shevchenko, P. Magnelind and M.Yu. Kupriyanov, "3D-MLSI: software package for inductance calculation in multilayer superconducting integrated circuits," *IEEE Trans. Appl. Supercond.*, vol.11, no. 1, 2001, p.1090.